How to cite: Angew. Chem. Int. Ed. 2024, e202318805
doi.org/10.1002/anie.202318805

DNA Nanotechnology

A Versatile Microfluidic Platform for Extravasation Studies Based on DNA Origami—Cell Interactions

Miguel García-Chamé, Parvesh Wadhwani, Juliana Pfeifer, Ute Schepers, Christof M. Niemeyer, and Carmen M. Domínguez**

Abstract: The adhesion of circulating tumor cells (CTCs) to the endothelial lumen and their extravasation to surrounding tissues are crucial in the seeding of metastases and remain the most complex events of the metastatic cascade to study. Integrins expressed on CTCs are major regulators of the extravasation process. This knowledge is primarily derived from animal models and biomimetic systems based on artificial endothelial layers, but these methods have ethical or technical limitations. We present a versatile microfluidic device to study cancer cell extravasation that mimics the endothelial barrier by using a porous membrane functionalized with DNA origami nanostructures (DONs) that display nanoscale patterns of adhesion peptides to circulating cancer cells. The device simulates physiological flow conditions and allows direct visualization of cell transmigration through microchannel pores using 3D confocal imaging. Using this system, we studied integrin-specific adhesion in the absence of other adhesive events. Specifically, we show that the transmigration ability of the metastatic cancer cell line MDA-MB-231 is influenced by the type, distance, and density of adhesion peptides present on the DONs. Furthermore, studies with mixed ligand systems indicate that integrins binding to RGD (arginine-glycine-aspartic acid) and IDS (isoleucine-aspartic acid-serine) did not synergistically enhance the extravasation process of MDA-MB-231 cells.

Introduction

Despite the inefficiency of circulating tumor cells (CTCs) to develop successful metastatic foci, metastasis remains the leading cause of >90% cancer deaths.[1] The complex metastatic journey of CTCs involves several stages and interactions, particularly with the endothelial cells that line blood vessels.[2] It begins when tumor cells detach from the primary tumor, intravasate into the bloodstream with the help of enzymatic degradation of the extracellular matrix (ECM), and navigate the circulatory system.[3] To survive this journey, CTCs resist shear forces and immune detection, often by aggregating or using platelets as a shield.[4] CTCs are then arrested within the vasculature of distant tissues through selectin- and integrin-mediated interactions, leading to increased adhesion to endothelial cells. This firm adhesion facilitates their extravasation by altering endothelial junctions and crossing the endothelial barrier into the tissue matrix, where they invade and establish new tumor sites.[5] Key molecular players in this process are integrins, which are essential for adhesion and invasion, chemokines and cytokines that direct tumor cell migration; and the ECM components, which can be remodeled to promote metastasis.[6] Among these steps, the extravasation of CTCs from the blood vessels is the most intricate stage to study, as it is a rare event that occurs within distant intact organs, and yet is poorly understood. Current understanding of extravasation derives mostly from intravital microscopy studies performed in animal models.[7] While these investigations have played a crucial role in recapitulating the pathophysiology behind metastasis, animal models imply economical, ethical, and translational limitations to human physiology[8] that have led to proposals for their complete elimination from preclinical research[9] and call for novel alternatives.

Microfluidic systems have emerged as a particularly convenient option to recapitulate the cellular interactions and physiological conditions during extravasation. They offer precise control over cellular components and the physicochemical environment, including essential mechan-

[*] M. García-Chamé, Prof. Dr. C. M. Niemeyer, Dr. C. M. Domínguez
Karlsruhe Institute of Technology (KIT)
Institute for Biological Interfaces 1 (IBG 1)
Hermann-von-Helmholtz-Platz
76344 Eggenstein-Leopoldshafen (Germany)
E-mail: christof.niemeyer@kit.edu
carmen.dominguez@kit.edu

Dr. P. Wadhwani
Karlsruhe Institute of Technology (KIT)
Institute for Biological Interfaces 2 (IBG 2)
Hermann-von-Helmholtz-Platz
76344 Eggenstein-Leopoldshafen (Germany)

J. Pfeifer, Prof. Dr. U. Schepers
Karlsruhe Institute of Technology (KIT)
Institute of Functional Interfaces (IFG)
Hermann-von-Helmholtz-Platz
76344 Eggenstein-Leopoldshafen (Germany)

ical cues, such as mimicking shear forces imposed by blood flow. These microfluidic devices are usually based on endothelial layers, immobilized on top of inert substrates or synthetic extracellular matrices, which cancer cells can use for adhesion and transmigration.[7] Recently, self-assembled vascular networks of endothelial cells have been applied to investigate extravasation.[7,10] Such systems have been successfully employed to evaluate, for instance, the effects that flow rates,[11] hypoxia,[12] substrate stiffness,[13] the presence of certain chemotactic agents,[14] or the glycocalyx[11a] have on the extravasation capabilities of different cancer cell lines. Despite their remarkable biomimetic level, the use of endothelial layers also poses technical challenges.[15] For example, protocols for coating engineered surfaces with adhesion proteins must be extensively optimized to ensure the growth of intact endothelial layers across the dimensions of the microfluidic channel.[16] Additionally, endothelial barrier quality assessments are required to verify permeability and adequate monolayer formation, and optimizing perfusion flow rates of the cell medium is essential to maintain the stability and viability of the cell barrier during the experimental time.[16b,17] Also, endothelial cells need a prior activation step to express membrane receptors for cell-cell interactions with cancer cells.[18] Most importantly, the use of endothelial layers does not allow the analytical system to study the effects of the type and nanoscale arrangement of specific biomolecules on the extravasation process. To overcome these limitations, we present here a generic microfluidic platform for extravasation studies that mimics the endothelial barrier by using a porous membrane decorated with DNA origami nanostructures (DONs) that display arrangements of selected adhesion peptides for circulating cancer cells.

DON-based technologies have recently emerged as a powerful tool for studying cell function in a controlled context. In contrast to conventional immobilization techniques for functionalizing surfaces with biomolecular ligands, DONs act as versatile molecular pegboards that enable precise stoichiometric control and geometric arrangement of functional ligands at the nanoscale.[19] This unique precision represents a significant advantage over conventional functionalization techniques, as it enables the creation of spatially defined ligand nanoarrays to mimic potential biological environments that cells may encounter. Due to the possibility of producing controlled patterns of ligands on length scales relevant to cell biology, this approach allows to modulate the spatial organization of ligand-receptor pairs to study the molecular mechanisms of cellular signal transduction processes through the resulting cellular responses. For example, DONs bearing ligands to target immunoglobulin-,[20] tyrosine kinase-,[20d,21] and tumor necrosis factor-receptors[22] have been reported to address questions about cell activation, motility, and apoptosis. Integrins, which play a role in cell motility in general,[23] and specifically in determining the sites at which adhesion to the endothelial lumen and extravasation occur,[6] have rarely been studied using DON-based methods. Few studies have addressed the use of DONs to interface integrins and modulate cell spreading, adhesion, and motility on flat surfaces,[21c,24] or to measure cellular mechanical forces.[25] However, to the best of our knowledge, the unique ability of DONs to produce nanoscale ligand architectures for the study of complex processes, such as cancer cell extravasation, has not been exploited. In this work, we demonstrate how ligand-modified DONs can be used within a cross-length-scale biomimetic chip platform to investigate the mechanistic basis for cancer cell extravasation processes. Specifically, we show how variations in two- and three-dimensional spatial arrangement, density, and combination of different integrin-binding peptides affect the extravasation efficiency of cancer cells under physiological flow conditions.

Results and Discussion

Our platform is based on the so-called vasQchip device, which was originally designed to mimic a blood vessel (Figure 1a) by allowing fluid flows that achieve physiologically relevant shear conditions.[26] The platform contains a semi-cylindrical polycarbonate (PC) microchannel (w: 0.35 mm×l: 20 mm) with cylindrical pores of about 8 μm in diameter that provide the physical space for cell extravasation. The microchannel is placed on top of a reservoir that contains medium to allow the capture of extravasated cells (Figures 1b and 1c). In this work, we took advantage of DNA nanotechnology to transform the vasQchip into an extravasation platform that presents peptide ligands for cellular adhesion in precise nanoscale arrangements, thereby mimicking the organization of adhesion ligands on the endothelial cell membrane (Figure 1d). To this end, we decorated the microchannel PC membrane with rectangular DONs with a size of $70\times100\,nm^2$ that were specifically modified to present peptide ligands (Figures 1e, 1f, S1, and S2) and included fluorescent dye labels (Cy3) to enable their optical detection. Based on previous work on DNA functionalization of microthermoformed 3D structures,[27] we functionalized the PC channel with GPTS (3-glycidyloxypropyl-trimethoxysilane), which bears epoxy-reactive groups to enable epoxy-amine crosslinking with amino-modified DNA capture oligonucleotides (see the Experimental Section for details on the functionalization). The DNA oligonucleotides tethered to the PC membrane then served as capture strands to hybridize with DONs containing complementary DNA strands protruding from their lower side (Figures 1d and S1).

Successful immobilization of DONs on the PC membrane was confirmed by confocal fluorescence microscopy, indicating strong Cy3 signals on the porous surface and inside the pores (Figures 2a and 2b). Through these signals, we confirmed a uniform distribution of DONs on the microchannel surface (Figure S3) with a density of 61 ± 12 DON/μm^2 (Figure S4), which was about 3 times higher than the density observed on planar glass surfaces;[21b,i] for details, see the Experimental Section. The DONs on the PC membrane were then functionalized with bioactive ligands using two common methods for DNA origami decoration: i) either by using chemically synthesized DNA-peptide conjugates that hybridized at precise locations defined by

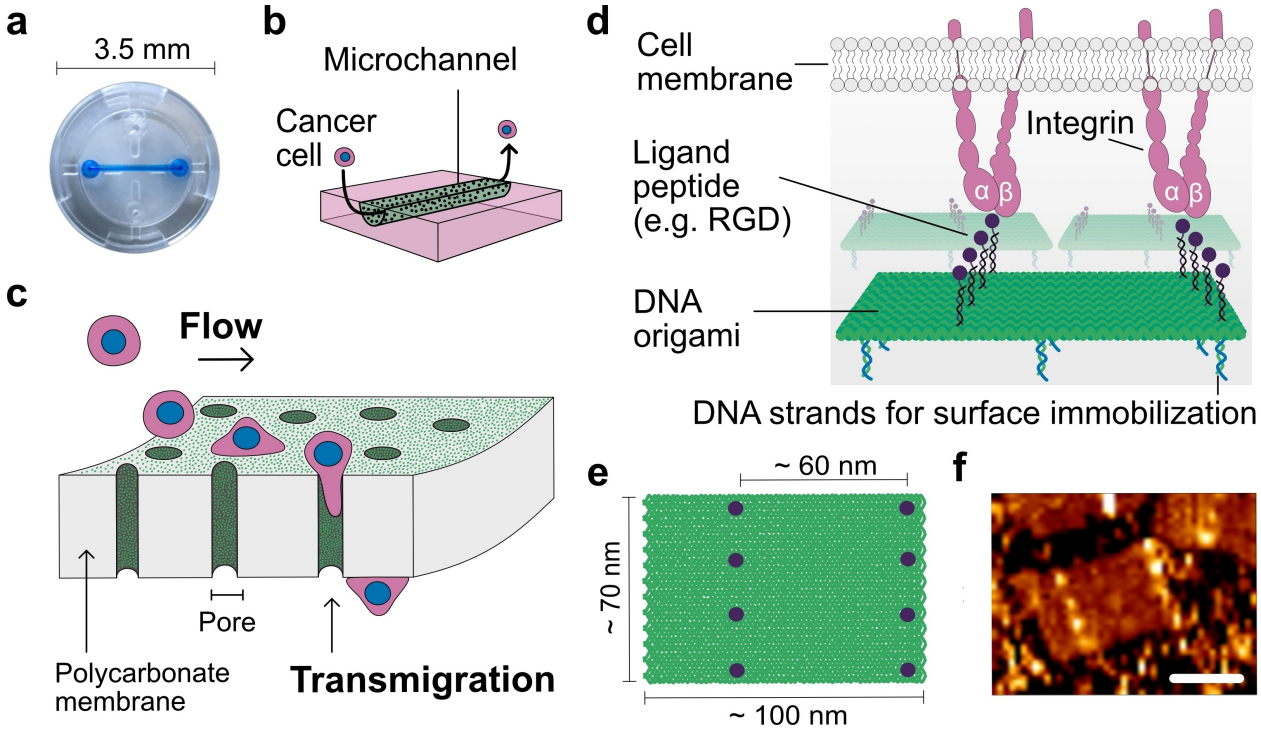

Figure 1. The microfluidic extravasation platform. **a)** VasQchip device with the porous PC microchannel (in blue). **b)** Scheme of cancer cells circulating through the microchannel. The chip allows the porous PC membrane to be placed on top of a reservoir to which cells could extravasate. **c)** Schematic representation of the transmigration of cancer cells through the porous membrane decorated with DONs presenting nanopatterns of adhesion ligands. **d)** RGD peptides as an example of an integrin-binding ligand used in this work to mimic the endothelial layer and induce cell adhesion to the porous flow channel. The DNA oligonucleotides tethered to the PC membrane served to immobilize DONs containing complementary DNA strands protruding from their lower side. **e)** Schematic top view of a DON containing a pattern of DNA-peptide conjugates arranged in two columns separated by 60 nm. Ligands in a column were spaced 15 nm apart from each other. **f)** AFM topographic image of the synthesized rectangular DONs with an approximate size of 70×100 nm. Here, the DON was decorated with DNA-STV conjugates to visualize the designed pattern, since the size of the adhesion peptides, such as RGD, is beyond the resolution limits of AFM imaging. Scale bar: 50 nm.

complementary DNA overhang strands protruding from the top of the DON, or ii) by using biotinylated peptides that were immobilized by streptavidin (STV) bridges (Figure S1). These strategies are two of the most common immobilization approaches for anchoring biomolecules to DNA nanostructures and allow to explore the effects of ligand flexibility and accessibility on the cellular response.[19e,20d,21h,28]

In this study, MDA-MB-231 human mammary adenocarcinoma cells served as the main working model due to their highly invasive nature and proven ability to metastasize in vitro.[7,29] Additionally, MCF-7 cells, which have lower motility than MDA-MB-231 cells,[30] were used to assess the platform functionality. Given the differences in integrin expression between MDA-MB-231 and MCF-7 cells, which likely influence their distinct biological behaviors,[31] we analyzed the results from each cell line independently.

In typical extravasation experiments, a suspension of cells was actively perfused through the microchannel using a peristaltic pump in a closed-loop circuit at a defined flow rate of 180 µL/min. A picture and schematics of the fluidic setup are shown in Figure S5. Under the applied flow rate, the maximum velocity reached in the center of the channel and the maximum shear stress found directly on the wall were ≈15 mm/s and ≈0.9 dynes/cm^2, respectively; as indicated by simulations of the fluid flow within the channel (Figure S6). These values correspond to the physiological stress experienced by cells inside veins and capillaries.[32] Confocal microscopy images of the microfluidic channel served to analyze whether cancer cells adhere and translocate through the functionalized pores (Figures 2c, 2d, and S7). To quantify extravasation events, we focused on the position of the nucleus because it is described as one of the most rigid organelles inside a cell.[33] Consequently, following transwell migration assays evaluation criteria,[34] successful transmigration of a cell was ascribed only when the cell nucleus had passed through a pore of the membrane and the cell had adhered to the outer wall of the microchannel. Cell extravasation was calculated as a percentage value using the number of transmigrated cells over the total number of cells found in 20 regions of interest of 212 µm×212 µm randomly selected.

To promote cell extravasation in our experiments, an FBS gradient was created between the two reservoirs by periodically perfusing FBS-enriched cell culture medium into the reservoir beneath the microchannel. Despite this gradient, initial experiments with both less invasive MCF-7 and metastatic MDA-MB-231 breast cancer epithelial cells

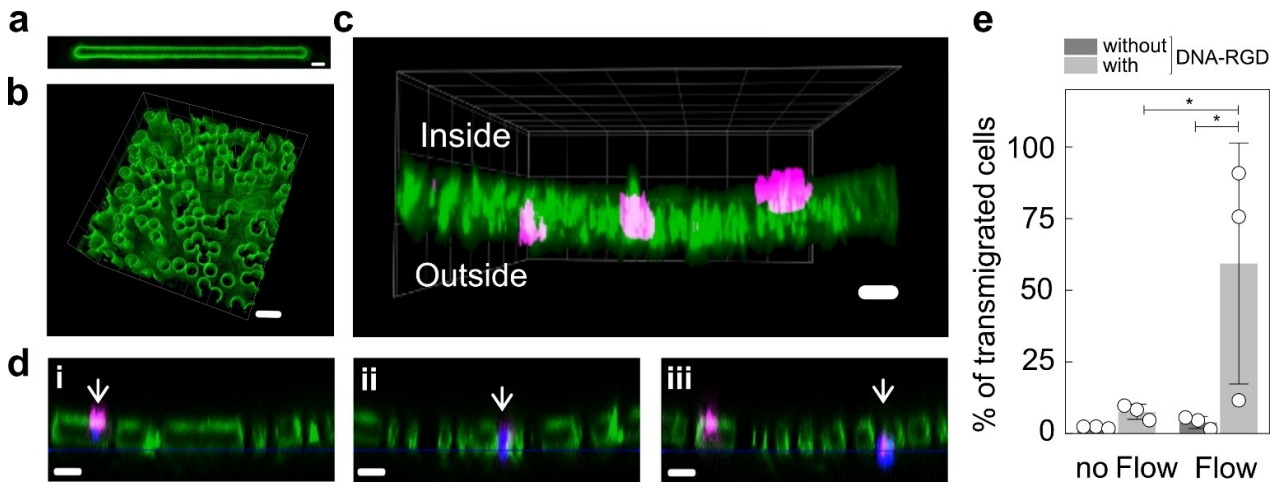

Figure 2. Visualization of cancer cell transmigration. **a)** The successful DON functionalization was indicated by fluorescence microscopy detection of Cy3-fluorescent DONs (in green) inside the PC microchannel. Scale bar: 2 mm. **b)** 3D microscopy image of the functionalized porous surface. Scale bar: 20 μm. **c)** 3D image of MDA-MB-231 cells in different positions across the microchannel walls. Actin filaments and nuclei of MDA-MB-231 cells were stained with Alexa Fluor 488 Phalloidin and Hoechst, respectively. Scale bar: 15 μm. **d)** The interaction of cells with the functionalized areas containing RGD-functionalized DONs resulted in three events: i) cells that did not enter the pores but are attached to the inner surface of the microchannel, ii) cells trapped in the pores, iii) cell transmigration through the pores of the PC membrane, as indicated by the position of the cell nucleus (in blue) on the outer face of the channel wall. Scale bars: 20 μm. **e)** Impact of flow conditions and adhesion ligands on the transmigration efficiency of MDA-MB-231 cells. The combination of flow and DNA-RGD conjugates was necessary to promote cell extravasation in our platform. P values were obtained from a two-way analysis of variance (ANOVA) test. *$P < 0.05$. All P values and details of statistical analysis are shown in Table S5.

revealed that fluid flow, and thus shear stress, was required to trigger extravasation in the first place (Figures 2e and S8). This observation aligns with earlier studies indicating that shear stress is a relevant factor that influences the ability of cancer cells to metastasize.[4,35] Technical limitations related to combining high-resolution imaging with the fluidic setup prevented real-time observation of extravasation under flow conditions. However, time-lapse images of extravasating cells recorded under static conditions (Figure S9) revealed migration times for MCF-7 and MDA-MB-231 cells of ≈3–5 μm/h, which agrees well with the reported range of 5.1 to 12.8 μm/h for cells crossing an endothelial barrier and moving through 15 μm wide channels.[36] Subsequent experiments were performed under flow to emulate the physiological conditions that promote cancer extravasation in vivo.

To validate the utility of the platform for extravasation studies, we tested it using DNA conjugates functionalized with the RGD peptide (arginine-glycine-aspartic acid). As discussed above, integrins are key players in cell adhesion and cancer cell extravasation.[5] Some integrins bind with high affinity to RGD tripeptides,[37] which are motifs found in proteins of the ECM;[37] but also in membrane proteins, such as certain IgCAMs,[5,38] crucial for cancer cell-endothelial cell interactions. Of particular interest are $\alpha_v\beta_3$ and $\alpha_5\beta_1$ integrins, involved in the first weak interactions and subsequent stabilization between tumor cells and the endothelium, respectively.[39] Both type of integrins bind to RGD peptides.[40] Initial experiments testing surfaces with DNA-RGD conjugates (for details on the synthesis of the DNA-peptide conjugates, see Experimental Section and Figure S10) demonstrated significantly enhanced transmigration efficiency under flow conditions for both MDA-MB-231 and MCF-7 cells, compared to surfaces without RGD, highlighting the role of RGD peptides in promoting cell transmigration. Notably, MDA-MB-231 cells showed a 20-fold higher transmigration efficiency in channels with DNA-RGD conjugates ($59.3 \pm 42\,\%$) compared to channels without RGD ($3.9 \pm 2.1\,\%$) (Figure 2e). These studies similarly showed that for MCF-7 cells (Figure S8), the presence of DNA-RGD conjugates was essential for triggering transmigration.

The platform also allowed the evaluation of cell morphology and proliferation after transmigration, as the growth of cells that had crossed the membrane and adhered to the reservoir under the microchannel could be easily tracked. We observed that MDA-MB-231 cells were still adhered to the outside of the membrane after 3 days (Figure S11a). Bright-field microscopy showed a seven-fold increase in cell number over 10 days with the characteristic morphology[41] maintained and cell viability $> 95\,\%$ (Figures 11b and 11c).

Having established that RGD peptides and shear stress effectively promote transmigration in our platform, we proceeded to study the effect of ligand arrangement and spacing on the extravasation capabilities of MDA-MB-231 cells. To this end, we first corroborated whether we could observe an effect on the transmigration efficiencies with varying distances between ligands. Previous studies suggest that the spacing between adhesion ligands has a significant role on the stability of cell adhesion on planar surfaces;[42] indicating that cell adhesion is favored by spacings < 60 nm between RGD motifs,[42c,d] and, more specifically, that integrin receptors are mainly distanced by 20–30 nm in clusters, as shown by super-resolution microscopy.[42e] There-

fore, to explore the effects on transmigration, we examined the impact of various spacings using DONs with DNA-RGD conjugates arranged at distances of 15, 30, 60, and 90 nm (Figure 3a). All results were compared to controls obtained with a reference DON lacking ligands, which served as a negative control to account for the non-specific adhesion of cancer cells to the DON (for details on all DON constructs used in this work, see Figures S2 and S12). Determination of transmigration efficiencies, carried out in triplicate experiments, indicated that surfaces decorated with 30 nm-spaced ligands (59.2 ± 28.6 %) led to a higher cellular transmigration than the reference control (5.7 ± 3.8 %), and appeared to be higher than those obtained with constructs bearing ligand columns spaced by 15 (35.3 ± 2.9 %), 60 (30.7 ± 16.4 %) or 90 nm (30.9 ± 12.2 %). These findings are in line with previous studies suggesting that integrins need optimal spacings between ligands to ensure high mechanical stability.[43] Based on these results, we considered the 30 nm spacing as an optimal distance to enhance cell transmigration in our assay and consequently performed all further experiments using this spacing.

Next, we investigated whether transmigration efficacy is affected by variations in the ligand system used to display the peptides on the DONs. The alternatives used here, DNA hybridization or STV-biotin interaction, aimed to reach conclusions on how the accessibility and flexibility of ligands influence transmigration. To this end, we designed a DON with two arrays of 4 adhesion ligands (8 ligands in total) separated by 30 nm in the x- and y-directions (Figures 3b, S2, and S12). Peptide attachment was achieved either by hybridization of DNA-peptide conjugates with oligonucleotides protruding from the DON plane (Figure 3b-i) or by STV-biotin bridges (Figure 3b-ii). For the latter, we used a bidentate biotin linker construct that allows for higher and more stable STV decoration, thereby enhancing the cellular response.[21h] Comparison of the transmigration events triggered by the different constructs revealed that DONs with DNA-RGD conjugates immobilized by DNA hybridization (21.9 ± 6.1 %) were more conducive to cellular transmigration than constructs containing the ligands via the less flexible STV-bridged display system (18.5 ± 1.6 %) (Figure 3b).

Integrins are a family of receptor heterodimers, comprising up to 24 members that differ from one another in characteristics, such as the adhesion ligands to which they respond. Although several integrins are sensitive to RGD, others are not.[44] $\alpha_4\beta_1$ integrins belong to this category and recognize IDS motifs (isoleucine-aspartic acid-serine) that are found in the membrane protein VCAM-1.[44b,45] Being currently an attractive candidate target for therapeutic drugs due to its crucial role in inflammatory diseases, cancer development, and metastasis;[44b,45–46] we aimed to use our

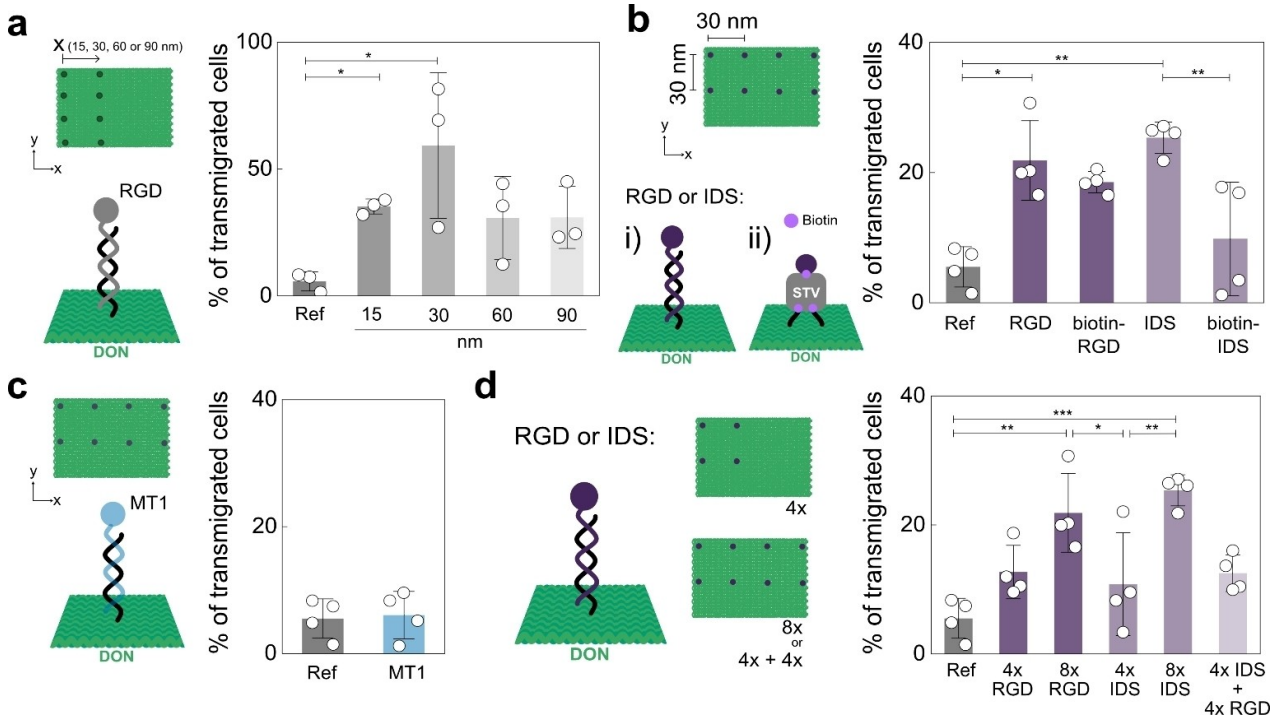

Figure 3. Effect of lateral spacing, type of adhesion peptide, ligand flexibility, and peptide density on the efficiency of cancer cell transmigration. **a)** Transmigration efficiency obtained with DONs presenting columns of DNA-RGD conjugates spaced by 15, 30, 60, or 90 nm. **b)** Comparison of the transmigration as a function of the ligand system used. i) RGD and IDS peptides were immobilized on DONs by direct DNA hybridization of DNA-peptide conjugates synthesized by Cu(I)-mediated 1,3-dipolar cycloaddition, or ii) by STV-biotin interactions using biotinylated peptides. The distances between ligands in the x and y directions were 30 nm. **c)** Transmigration efficiency obtained with DON bearing eight DNA-MT1 conjugates arranged with spacings of 30 nm in the x- and y-directions. **d)** Transmigration efficiency as a function of the ligand density and combination of RGD and IDS ligands. P values were obtained from two sample t- or Kruskal-Wallis tests. *P < 0.05, **P < 0.01, ***P < 0.001. All P values and details of statistical analysis are provided in Table S5.

platform to investigate whether activation of $\alpha_4\beta_1$ integrins with IDS peptides is also associated with cancer cell extravasation. To this end, we prepared covalently linked DNA-IDS peptide conjugates as well as biotinylated IDS peptides for STV-mediated immobilization (Figure S10). Using these reagents in analogous experiments as described above (Figure 3b), we observed that channels with DON decorated with DNA-IDS conjugates resulted in a higher transmigration efficiency ($25.4 \pm 2.4\,\%$) than those with DON containing biotin-IDS constructs ($9.8 \pm 8.7\,\%$). The latter were practically indistinguishable from those of the reference control without ligands ($5.5 \pm 3.1\,\%$). From a biological point of view, it is interesting that IDS led to a comparably high increase in transmigration as RGD. From a technical point of view in relation to the display platform, these results show that flexible presentation by direct conjugates leads to a stronger biological effect, which is probably due to improved steric accessibility as a result of the greater distance and/or flexibility of the DNA linker. It can be estimated that peptides immobilized by DNA hybridization are separated vertically by ≈ 8 nm from the DON surface, whereas the distance should be shorter in the case of STV bridges (STV diameter ≈ 5 nm).[47]

After the initial investigations of integrins, we also aimed to examine other receptors that influence the metastatic process but are not related to mediating cell attachment. It is widely accepted that extravasation coincides with places where the glycocalyx of endothelial cells is degraded. This degradation is produced by the metalloproteinase MMP2 and its expression is activated by the membrane metalloproteinase MT1-MMP.[48] These cellular receptors are activated in a similar manner to integrins and both have shown cooperation at membrane protrusions (filopodia and lamellipodia) and at cell-cell junctions, jointly regulating cell motility.[49] To target the MT1-MMP, we used the peptide HWKHLHNTKTFL (hereinafter referred to as MT1) that binds to the "MT-Loop" region with high affinity.[50] To investigate potential effects of MT1 on the extravasation, DNA-MT1 conjugates were prepared similar to IDS- and RGD-DNA conjugates (Figure S10), and transmigration efficiency was analyzed as described above. We found that channels with DONs bearing MT1 peptides ($6.1 \pm 3.7\,\%$) were not sufficient to promote extravasation, as the response did not differ from the reference control (Figure 3c). Therefore, although the metalloproteinase targeted by this peptide promotes extravasation by contributing to the degradation of the ECM,[48a] this receptor alone appears not to favor a firm cell adhesion to initiate cell transmigration in our assay.

Overall, the above results show that our platform allows us to study ligand-dependent adhesion and extravasation processes individually for different bioactive ligands and independently of other cell-cell interaction events. However, compared to other in vitro methods, our DON-based approach also allows to specifically analyze the stoichiometry and nanoscale architecture of different ligand displays. For example, to address how the density of adhesion peptides would influence cell transmigration response, we prepared DONs with only 4 adhesion ligands (Figure 3d). As expected, the transmigration response in channels presenting 4×DNA-RGD conjugates ($12.7 \pm 4.1\,\%$) was lower than in those with 8×DNA-RGD ($21.9 \pm 6.1\,\%$). Similarly, the transmigration efficiency in channels containing DONs with 4×DNA-IDS ($10.8 \pm 7.9\,\%$) was lower than the DONs modified with 8×DNA-IDS ($25.4 \pm 2.4\,\%$). These results showed that the number of ligands per DON has an impact on the cell response, which agrees with previous studies on other platforms.[20a,f–i,21c,g]

To investigate whether nanoscale arrangements of different ligands affect cell extravasation, we next designed a DON for the simultaneous display of 4×DNA-IDS and 4×DNA-RGD conjugates. To ensure orthogonal decoration with the same hybridization efficiency for both DNA-peptide conjugates, we used the same prominent oligonucleotide sequence but in different directions (5′–3′ and 3′–5′) for the immobilization of the two ligands on the DON. Our results showed no enhanced transmigration effect by the combination of IDS and RGD ligands targeting different integrin heterodimers. The observed response ($12.5 \pm 2.9\,\%$) was consistent with the transmigration efficiency of DONs with either only 4 DNA-RGD or only 4 DNA-IDS conjugates (Figure 3d). This suggests that although IDS and RGD individually promote cell migration, their presence together did not confer additional benefits, indicating a limited cooperative role when both ligands are present in combination. Previous works have suggested a synergistic enhancement in the adhesion[51] and changes in migration speed[52] on planar surfaces for mixed ligands targeting $\alpha_2\beta_1$ and $\alpha_5\beta_1$[51] or $\alpha_v\beta_3$ and $\alpha_5\beta_1$[52] integrins. However, it is unclear whether there is a cooperative effect between $\alpha_v\beta_3$ and $\alpha_5\beta_1$ integrins for cell extravasation, and our system could not be used for this purpose because both receptors recognize the RGD ligand we used, and therefore cannot be distinguished in our studies. Although recent attention has been paid to possible synergies between these and $\alpha_4\beta_1$ integrins (which recognize IDS), as they play an individual role in the complicated cascade of cancer cell extravasation,[46b,53] synergistic effects between them have not yet been investigated. Therefore, the results obtained here should be taken as preliminary evidence to suggest that integrins responsive to IDS ($\alpha_4\beta_1$) and RGD (e.g., $\alpha_5\beta_1$ and $\alpha_v\beta_3$) peptides exhibit limited synergistic effects in enhancing cellular extravasation. These results are in line with previous studies indicating limited cooperation of integrins. Therein, experiments combining $\alpha_v\beta_3$, $\alpha_2\beta_1$ and $\alpha_3\beta_1$ with two integrin-binding peptides at variable molar ratios in polysaccharide matrices did not reveal significant differences in cell adhesion for various combinations.[54] Taken together, our findings highlight the complexity of studying the broad spectrum of integrin-ligand interactions, underscoring the need to investigate the effects of ligand combination and organization with nanoscale molecular resolution under physiologically relevant conditions. Our platform enables the presentation of ligands with control over density and stoichiometry, which is critical for the study of interactions between different ligand subtypes. In particular, the ability to immobilize peptide ligands that specifically bind to different receptor subtypes represents a major advance, as it avoids the disruptive effects that can arise, for example,

from multiple integrin binding sites in native proteins on endothelial cell layers.

Although there are still technical obstacles to overcome resulting from high-resolution imaging under flow conditions, such as focus drift and light diffusion caused by the cell culture medium and membrane pores blurring the edges of the membrane (Figure S9a); this platform opens up the possibility to monitor the transmigration of cancer cells through porous membranes in real-time. Thus, our platform, despite current live imaging limitations, holds significant potential for combining DNA nanostructure-based microfluidic assays with advanced microscopy, promising to be a valuable tool in cell extravasation research.

Conclusion

We have developed a microfluidic platform to recapitulate the interactions between cancer cell receptors and their ligands in the context of cancer cell extravasation. Our device mimics two key features of blood vessels: fluid flow to emulate the physiological shear stress imposed by the bloodstream, and adhesion peptides displayed on the channel's lumen. The device has a porous fluidic channel that can be functionalized with DNA nanostructures bearing selected nanopatterns of adhesion ligands. Using this platform, we could characterize quantitatively how variations in the organization, spacing, type, density, and combination of the different RGD and IDS integrin binding peptides impact the extravasation efficiency of MDA-MB-231 cells. We found that the integrin biding ligands induced cell transmigration in a stoichiometry-dependent manner. Furthermore, we revealed that a combination of RGD and IDS ligands simultaneously on the same DON did not show a synergistic effect in promoting extravasation. Lateral spacing between adhesion ligands of 30 nm and flexible DNA-peptide conjugates favored cell translocation. We also obtained evidence that ligand interactions between receptors that are not involved in cell adhesion, but play a central role in controlling cancer cell invasiveness by degrading the endothelial barrier in the pre-metastatic niche, such as the MT1-MMP receptor and MT1 ligand system studied here, do not directly contribute to cell extravasation.

The platform presented here should provide a viable alternative to traditional extravasation testing, as it avoids the technical challenges of using intact endothelial layers while offering the advantages of greater simplicity and versatility. Our method not only allows the investigation of integrin-specific adhesion in the absence of other adhesion events and the direct visualization of ligand-specific binding events in cancer cell transmigration, but can be transferred to other ligands. Hence, the technology can open the door to advanced studies with other types of cells, such as CTCs derived from cancer patients, which could be highly relevant models, as adaptation of CTCs to blood flow can induce traits that are not present in established cell lines. Since the extravasated cells could be recovered from the chip, genetic analyses could provide information on whether contact with certain ligands and the mechanical passage induces changes in gene expression in standard cancer cell lines or CTCs. We anticipate that this versatile platform will become a valuable tool to study extravasation with controlled nanoscale molecular patterns, thereby helping to unravel the fundamentals of the metastatic process and identify new therapeutic approaches to attenuate metastasis.

Supporting Information

The authors have cited additional references within the Supporting Information.[21h,26,47,55]

Acknowledgements

This work was financially supported through the Research Seed Capital program (RiSC) of the Ministerium für Wissenschaft, Forschung und Kunst Baden-Württemberg (MWK BW); the Helmholtz program "Materials Systems Engineering" under the topic "Adaptive and Bioinstructive Materials Systems"; the Deutsche Forschungsgemeinschaft (DFG, German Research Foundation) under Germany's Excellence Strategy via the Excellence Cluster "3D Matter Made to Order" (3DMM2O, EXC-2082/1-390761711, Thrusts C3) and the DFG Research Training Group 2039. The authors acknowledge fruitful discussions with Ada Cavalcanti-Adam and Jonathan P. Sleeman, and lab support by Hannah Buntz, Tamara Molitor and Alexander Bruckmann. Open Access funding enabled and organized by Projekt DEAL.

Conflict of Interest

The authors declare no conflict of interest.

Keywords: cancer · DNA structures · extravasation · integrins · microfluidics

[1] K. Ganesh, J. Massague, *Nat. Med.* **2021**, *27*, 34.
[2] J. Massagué, A. C. Obenauf, *Nature* **2016**, *529*, 298.
[3] Z. Elgundi, M. Papanicolaou, G. Major, T. R. Cox, J. Melrose, J. M. Whitelock, B. L. Farrugia, *Front. Oncol.* **2020**, *9*, 1482.
[4] E. S. Ildiz, A. Gvozdenovic, W. J. Kovacs, N. Aceto, *Clin. Exp. Metastasis* **2023**, *40*, 375.
[5] G. Sokeland, U. Schumacher, *Mol. Cancer* **2019**, *18*, 12.
[6] J. Fares, M. Y. Fares, H. H. Khachfe, H. A. Salhab, Y. Fares, *Signal Transduct Target Theraphy* **2020**, *5*, 28.
[7] M. F. Coughlin, R. D. Kamm, *Adv. Healthcare Mater.* **2020**, *9*, e1901410.
[8] D. E. Ingber, *Nat. Rev. Genet.* **2022**, *23*, 467.
[9] a) H. Ledford, *Nature* **2011**, *477*, 526; b) S. B. Gorzalczany, A. G. Rodriguez Basso, *Pharmacol. Res. Perspect.* **2021**, *9*, e00863.
[10] S. Kim, Z. Wan, J. S. Jeon, R. D. Kamm, *Front. Oncol.* **2022**, *12*, 1052192.
[11] a) C. Hajal, L. Ibrahim, J. C. Serrano, G. S. Offeddu, R. D. Kamm, *Biomaterials* **2021**, *265*, 120470; b) J. Yu, S. Lee, J.

Song, S. R. Lee, S. Kim, H. Choi, H. Kang, Y. Hwang, Y. K. Hong, N. L. Jeon, *Nano Convergence* **2022**, *9*, 16.
[12] J. Song, A. Miermont, C. T. Lim, R. D. Kamm, *Sci. Rep.* **2018**, *8*, 17949.
[13] S. Azadi, M. Tafazzoli Shadpour, M. E. Warkiani, *Biotechnol. Bioeng.* **2021**, *118*, 823.
[14] H. Y. Cho, J. H. Choi, K. J. Kim, M. Shin, J. W. Choi, *Front Bioeng Biotechnol* **2020**, *8*, 611802.
[15] a) S. Schneider, D. Gruner, A. Richter, P. Loskill, *Lab Chip* **2021**, *21*, 1866; b) H. Kutluk, E. E. Bastounis, I. Constantinou, *Adv. Healthcare Mater.* **2023**, *12*, e2203256.
[16] a) C. M. Sakolish, M. B. Esch, J. J. Hickman, M. L. Shuler, G. J. Mahler, *e-biomed* **2016**, *5*, 30; b) C. M. Leung, P. de Haan, K. Ronaldson-Bouchard, G.-A. Kim, J. Ko, H. S. Rho, Z. Chen, P. Habibovic, N. L. Jeon, S. Takayama, M. L. Shuler, G. Vunjak-Novakovic, O. Frey, E. Verpoorte, Y.-C. Toh, *Nat. Rev. Methods Primers* **2022**, *2*, 33.
[17] a) Y. B. Arik, M. W. van der Helm, M. Odijk, L. I. Segerink, R. Passier, A. van den Berg, A. D. van der Meer, *Biomicrofluidics* **2018**, *12*, 042218; b) L. Lin, X. Wang, M. Niu, Q. Wu, H. Wang, Y. Zu, W. Wang, *Engineered Regeneration* **2022**, *3*, 201.
[18] M. K. Shin, S. K. Kim, H. Jung, *Lab Chip* **2011**, *11*, 3880.
[19] a) C. M. Niemeyer, *Angew. Chem. Int. Ed.* **2010**, *49*, 1200; b) B. Sacca, C. M. Niemeyer, *Angew. Chem. Int. Ed.* **2012**, *51*, 58; c) A. K. Schneider, C. M. Niemeyer, *Angew. Chem. Int. Ed.* **2018**, *57*, 16959; d) S. Mishra, Y. Feng, M. Endo, H. Sugiyama, *ChemBioChem* **2020**, *21*, 33; e) G. A. Knappe, E. C. Wamhoff, M. Bathe, *Nat. Rev. Mater.* **2023**, *8*, 123.
[20] a) R. Veneziano, T. J. Moyer, M. B. Stone, E. C. Wamhoff, B. J. Read, S. Mukherjee, T. R. Shepherd, J. Das, W. R. Schief, D. J. Irvine, M. Bathe, *Nat. Nanotechnol.* **2020**, *15*, 716; b) J. Hellmeier, R. Platzer, A. S. Eklund, T. Schlichthaerle, A. Karner, V. Motsch, M. C. Schneider, E. Kurz, V. Bamieh, M. Brameshuber, J. Preiner, R. Jungmann, H. Stockinger, G. J. Schutz, J. B. Huppa, E. Sevcsik, *Proc. Natl. Acad. Sci. USA* **2021**, *118*, e2016857118; c) T. Fang, J. Alvelid, J. Spratt, E. Ambrosetti, I. Testa, A. I. Teixeira, *ACS Nano* **2021**, *15*, 3441; d) G. A. O. Cremers, B. Rosier, A. Meijs, N. B. Tito, S. M. J. van Duijnhoven, H. van Eenennaam, L. Albertazzi, T. F. A. de Greef, *J. Am. Chem. Soc.* **2021**, *143*, 10131; e) J. Hellmeier, R. Platzer, V. Muhlgrabner, M. C. Schneider, E. Kurz, G. J. Schutz, J. B. Huppa, E. Sevcsik, *ACS Nano* **2021**, *15*, 15057; f) R. Dong, T. Aksel, W. Chan, R. N. Germain, R. D. Vale, S. M. Douglas, *Proc. Natl. Acad. Sci. USA* **2021**, *118*, e2109057118; g) C. H. Wang, X. Q. Chen, Y. Y. Su, H. Wang, D. Li, *Chin. J. Anal. Chem.* **2022**, *50*, 100091; h) Y. Sun, J. Sun, M. Xiao, W. Lai, L. Li, C. Fan, H. Pei, *Sci. Adv.* **2022**, *8*, eadd1106; i) L. Schneider, K. S. Rabe, C. M. Dominguez, C. M. Niemeyer, *ACS Nano* **2023**, *17*, 6719; j) K. F. Wagenbauer, N. Pham, A. Gottschlich, B. Kick, V. Kozina, C. Frank, D. Trninic, P. Stommer, R. Grunmeier, E. Carlini, C. A. Tsiverioti, S. Kobold, J. J. Funke, H. Dietz, *Nat. Nanotechnol.* **2023**, *18*, 1319; k) J. Hellmeier, R. Platzer, J. B. Huppa, E. Sevcsik, in *The Immune Synapse: Methods and Protocols, Vol. 2654* (Eds.: C. T. Baldari, M. L. Dustin), Springer US, New York, NY **2023**, pp. 277.
[21] a) A. Shaw, V. Lundin, E. Petrova, F. Fordos, E. Benson, A. Al-Amin, A. Herland, A. Blokzijl, B. Hogberg, A. I. Teixeira, *Nat. Methods* **2014**, *11*, 841; b) A. Angelin, S. Weigel, R. Garrecht, R. Meyer, J. Bauer, R. K. Kumar, M. Hirtz, C. M. Niemeyer, *Angew. Chem. Int. Ed.* **2015**, *54*, 15813; c) D. Huang, K. Patel, S. Perez-Garrido, J. F. Marshall, M. Palma, *ACS Nano* **2019**, *13*, 728; d) Y. Hu, C. M. Dominguez, S. Christ, C. M. Niemeyer, *Angew. Chem. Int. Ed.* **2020**, *59*, 19016; e) P. Lanzerstorfer, U. Müller, K. Gordiyenko, J. Weghuber, C. M. Niemeyer, *Biomol. Eng.* **2020**, *10*, 540; f) T. Verheyen, T. Fang, D. Lindenhofer, Y. Wang, K. Akopyan, A. Lindqvist, B. Hogberg, A. I. Teixeira, *Nucleic Acids Res.* **2020**, *48*, 5777; g) M. Wang, D. Yang, Q. Lu, L. Liu, Z. Cai, Y. Wang, H. H. Wang, P. Wang, Z. Nie, *Nano Lett.* **2022**, *22*, 8445; h) C. M. Dominguez, M. Garcia-Chame, U. Muller, A. Kraus, K. Gordiyenko, A. Itani, H. Haschke, P. Lanzerstorfer, K. S. Rabe, C. M. Niemeyer, *Small* **2022**, *18*, e2202704; i) I. Mayer, T. Karimian, K. Gordiyenko, A. Angelin, R. Kumar, M. Hirtz, R. Mikut, M. Reischl, J. Stegmaier, L. Zhou, R. Ma, G. U. Nienhaus, K. S. Rabe, P. Lanzerstorfer, C. M. Domínguez, C. M. Niemeyer, *Nano Lett.* **2024**, *24*, 1611.
[22] a) Y. Wang, I. Baars, F. Fordos, B. Hogberg, *ACS Nano* **2021**, *15*, 9614; b) R. M. L. Berger, J. M. Weck, S. M. Kempe, O. Hill, T. Liedl, J. O. Radler, C. Monzel, A. Heuer-Jungemann, *Small* **2021**, *17*, e2101678.
[23] Y. A. Kadry, D. A. Calderwood, *Biochim. Biophys. Acta Biomembr.* **2020**, *1862*, 183206.
[24] a) D. Karna, M. Stilgenbauer, S. Jonchhe, K. Ankai, I. Kawamata, Y. Cui, Y. R. Zheng, Y. Suzuki, H. Mao, *Bioconjugate Chem.* **2021**, *32*, 311; b) A. Buchberger, K. Riker, J. Bernal-Chanchavac, R. P. Narayanan, C. R. Simmons, N. E. Fahmi, R. Freeman, N. Stephanopoulos, *ACS Appl. Bio Mater.* **2022**, *5*, 4625.
[25] a) P. K. Dutta, Y. Zhang, A. T. Blanchard, C. Ge, M. Rushdi, K. Weiss, C. Zhu, Y. Ke, K. Salaita, *Nano Lett.* **2018**, *18*, 4803; b) A. Mills, N. Aissaoui, D. Maurel, J. Elezgaray, F. Morvan, J. J. Vasseur, E. Margeat, R. B. Quast, J. Lai Kee-Him, N. Saint, C. Benistant, A. Nord, F. Pedaci, G. Bellot, *Nat. Commun.* **2022**, *13*, 3182; c) H. Matsubara, H. Fukunaga, T. Saito, K. Ikezaki, M. Iwaki, *ACS Nano* **2023**, *17*, 13185.
[26] V. Kappings, C. Grün, D. Ivannikov, I. Hebeiss, S. Kattge, I. Wendland, B. E. Rapp, M. Hettel, O. Deutschmann, U. Schepers, *Adv. Mater. Technol.* **2018**, *3*, 1700246.
[27] A. K. Schneider, P. M. Nikolov, S. Giselbrecht, C. M. Niemeyer, *Small* **2017**, *13*, 1603923.
[28] A. Comberlato, M. M. Koga, S. Nüssing, I. A. Parish, M. M. C. Bastings, *Nano Lett.* **2022**, *22*, 2506.
[29] R. Driver, S. Mishra, *BioChip J.* **2022**, *17*, 1.
[30] a) H. Eslami Amirabadi, M. Tuerlings, A. Hollestelle, S. SahebAli, R. Luttge, C. C. van Donkelaar, J. W. M. Martens, J. M. J. den Toonder, *Biomed. Microdevices* **2019**, *21*, 101; b) T. Fischer, A. Hayn, C. T. Mierke, *Front Cell Dev Biol* **2020**, *8*, 393.
[31] a) A. Taherian, X. Li, Y. Liu, T. A. Haas, *BMC Cancer* **2011**, *11*, 293; b) M.-R. Hermann, M. Jakobson, G. P. Colo, E. Rognoni, M. Jakobson, C. Kupatt, G. Posern, R. Fässler, *J. Cell Sci.* **2016**, *129*, 1391.
[32] D. C. Fernandes, T. L. S. Araujo, F. R. M. Laurindo, L. Y. Tanaka, in *Endothelium and Cardiovascular Diseases* (Eds.: P. L. Da Luz, P. Libby, A. C. P. Chagas, F. R. M. Laurindo), Academic Press **2018**, pp. 85.
[33] Q. Feng, B. Kornmann, *J. Cell Sci.* **2018**, *131*, jcs218479.
[34] a) J. Marshall, in *Cell Migration: Developmental Methods and Protocols* (Eds.: C. M. Wells, M. Parsons), Humana Press, Totowa, NJ **2011**, pp. 97; b) A. F. van de Merbel, G. van der Horst, J. T. Buijs, G. van der Pluijm, in *Prostate Cancer: Methods and Protocols, Vol. 1786* (Ed.: Z. Culig), Springer New York, New York, NY **2018**, pp. 67; c) C. R. Justus, M. A. Marie, E. J. Sanderlin, L. V. Yang, *Methods Mol. Biol.* **2023**, *2644*, 349.
[35] a) S. Ma, A. Fu, G. G. Chiew, K. Q. Luo, *Cancer Lett.* **2017**, *388*, 239; b) G. Follain, D. Herrmann, S. Harlepp, V. Hyenne, N. Osmani, S. C. Warren, P. Timpson, J. G. Goetz, *Nat. Rev. Cancer* **2020**, *20*, 107.
[36] S. A. Roberts, A. E. Waziri, N. Agrawal, *Anal. Chem.* **2016**, *88*, 2770.

[37] B. S. Ludwig, H. Kessler, S. Kossatz, U. Reuning, *Cancers* **2021**, *13*, 1711.
[38] B. LaFoya, J. A. Munroe, A. Miyamoto, M. A. Detweiler, J. J. Crow, T. Gazdik, A. R. Albig, *Int. J. Mol. Sci.* **2018**, *19*, 449.
[39] N. Osmani, G. Follain, M. J. Garcia Leon, O. Lefebvre, I. Busnelli, A. Larnicol, S. Harlepp, J. G. Goetz, *Cell Rep.* **2019**, *28*, 2491.
[40] L. A. Rocha, D. A. Learmonth, R. A. Sousa, A. J. Salgado, *Biotechnol. Adv.* **2018**, *36*, 208.
[41] atcc.org, *MDA-MB-231*, https://www.atcc.org/products/htb-26.
[42] a) J. Huang, S. V. Grater, F. Corbellini, S. Rinck, E. Bock, R. Kemkemer, H. Kessler, J. Ding, J. P. Spatz, *Nano Lett.* **2009**, *9*, 1111; b) M. J. Paszek, D. Boettiger, V. M. Weaver, D. A. Hammer, *PLoS Comput. Biol.* **2009**, *5*, e1000604; c) M. Schvartzman, M. Palma, J. Sable, J. Abramson, X. Hu, M. P. Sheetz, S. J. Wind, *Nano Lett.* **2011**, *11*, 1306; d) V. Schaufler, H. Czichos-Medda, V. Hirschfeld-Warnecken, S. Neubauer, F. Rechenmacher, R. Medda, H. Kessler, B. Geiger, J. P. Spatz, E. A. Cavalcanti-Adam, *Cell Adhes. Migr.* **2016**, *10*, 505; e) T. Schlichthaerle, C. Lindner, R. Jungmann, *Nat. Commun.* **2021**, *12*, 2510.
[43] a) Z. Sun, M. Costell, R. Fassler, *Nat. Cell Biol.* **2019**, *21*, 25; b) S. Zheng, Q. Liu, J. He, X. Wang, K. Ye, X. Wang, C. Yan, P. Liu, J. Ding, *Nano Res.* **2022**, *15*, 1623.
[44] a) R. De Marco, A. Tolomelli, E. Juaristi, L. Gentilucci, *Med. Res. Rev.* **2016**, *36*, 389; b) J. Zhao, F. Santino, D. Giacomini, L. Gentilucci, *Biomedicine* **2020**, *8*, 307.
[45] J. H. Wang, R. B. Pepinsky, T. Stehle, J. H. Liu, M. Karpusas, B. Browning, L. Osborn, *Proc. Natl. Acad. Sci. USA* **1995**, *92*, 5714.
[46] a) R. De Marco, A. Greco, N. Calonghi, S. D. Dattoli, M. Baiula, S. Spampinato, P. Picchetti, L. De Cola, M. Anselmi, F. Cipriani, L. Gentilucci, *Biopolymers* **2017**, *110*, e23081; b) M. Baiula, S. Spampinato, L. Gentilucci, A. Tolomelli, *Front. Chem.* **2019**, *7*, 489.
[47] S. Avvakumova, M. Colombo, E. Galbiati, S. Mazzucchelli, R. Rotem, D. Prosperi, in *Biomedical Applications of Functionalized Nanomaterials* (Eds.: B. Sarmento, J. das Neves), Elsevier **2018**, pp. 139.
[48] a) S. Niland, J. A. Eble, *Int. J. Mol. Sci.* **2021**, *22*, 238; b) D. V. Maybee, N. L. Ink, M. A. M. Ali, *Int. J. Mol. Sci.* **2022**, *23*, 9513.
[49] P. Gonzalo, V. Moreno, B. G. Galvez, A. G. Arroyo, *BioFactors* **2010**, *36*, 248.
[50] L. Zhu, H. Wang, L. Wang, Y. Wang, K. Jiang, C. Li, Q. Ma, S. Gao, L. Wang, W. Li, M. Cai, H. Wang, G. Niu, S. Lee, W. Yang, X. Fang, X. Chen, *J. Controlled Release* **2011**, *150*, 248.
[51] C. D. Reyes, T. A. Petrie, A. J. Garcia, *J. Cell. Physiol.* **2008**, *217*, 450.
[52] J. L. Young, X. Hua, H. Somsel, F. Reichart, H. Kessler, J. P. Spatz, *Nano Lett.* **2020**, *20*, 1183.
[53] a) H. Laubli, L. Borsig, *Front. Immunol.* **2019**, *10*, 2120; b) M. Li, Y. Wang, M. Li, X. Wu, S. Setrerrahmane, H. Xu, *Acta Pharm. Sin. B* **2021**, *11*, 2726.
[54] K. Hozumi, C. Fujimori, F. Katagiri, Y. Kikkawa, M. Nomizu, *Biomaterials* **2015**, *37*, 73.
[55] a) H. K. Walter, J. Bauer, J. Steinmeyer, A. Kuzuya, C. M. Niemeyer, H. A. Wagenknecht, *Nano Lett.* **2017**, *17*, 2467; b) R. Wacker, C. M. Niemeyer, *Curr. Protoc. Nucleic Acid Chem.* **2005**, *12*, 12.7.1.

Manuscript received: December 7, 2023
Accepted manuscript online: April 30, 2024
Version of record online: ■■, ■■

Research Articles

DNA Nanotechnology

M. García-Chamé, P. Wadhwani, J. Pfeifer, U. Schepers, C. M. Niemeyer,* C. M. Domínguez* _____ e202318805

A Versatile Microfluidic Platform for Extravasation Studies Based on DNA Origami—Cell Interactions

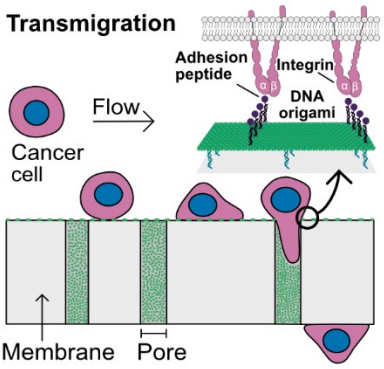

Microfluidic device to study cancer cell extravasation that mimics the endothelial barrier using a porous membrane decorated with DNA origami nanostructures displaying adhesion peptides to circulating cancer cells. The device allows visualization of cell transmigration under physiological flow conditions, revealing influences of adhesion peptide type, spatial arrangement, and density on the extravasation of MDA-MB-231 cells.